ORIGINAL PAPER

CrossMark

Measurement of T_{1e}, T_{1N}, T_{1HE}, T_{2e}, and T_{2HE} by Pulse EPR at X-Band for Nitroxides at Concentrations Relevant to Solution DNP

Joshua R. Biller[1,3] · Joseph E. McPeak[2] · Sandra S. Eaton[2] · Gareth R. Eaton[2]

Abstract

Relaxation times were measured at X-band (9.5 GHz) at concentrations up to 20.8 mM for two nitroxides that are widely used in Overhauser dynamic nuclear polarization (ODNP) experiments. Carboxy proxyl (CP, 3-carboxy-2,2,5,5-tetramethyl-1-pyrrolidinyloxy) in water and tempol (TP, 4-hydroxy-2,2,6,6-tetramethylpiperidin-1-oxyl) in toluene have been studied with oxygen removed. For comparison, solutions of CP were also studied in air-saturated solution, which is the typical preparation for ODNP experiments. T_2 and T_{2HE} (HE = Heisenberg exchange) were measured by electron spin echo. The spin magnetization recovery time constant from inversion recovery experiments, which we denote as T_{1e}^*, includes contributions from T_{1e} and T_{1HE}. In the absence of oxygen, values of T_{1e}^* for both radicals decrease with increasing concentration up to ~1 mM, then increase again towards 10 mM. The concentration dependence results from changes in the relative contributions from T_{1e} and T_{1HE}. In air-saturated solutions of CP T_{1e}^* decreases with concentration to about 200 ns at 1 mM, and then remains independent of further concentration increases. T_{1e} and T_{1N} were also measured with a digital saturation recovery spectrometer. Using the combined results from spin echo, inversion recovery, and saturation recovery we could extract the values of T_{1e}, T_{1HE}, T_{1N}, T_{2e}, and T_{2HE} for both radicals in this fast tumbling regime.

Certain commercial instruments and software are identified to specify the experimental study adequately. This does not imply endorsement by NIST or that the instruments and software are the best available for the purpose.

✉ Joshua R. Biller
  Joshua.biller@nist.gov; jbiller@tda.com

Extended author information available on the last page of the article

1 Introduction

Solution dynamic nuclear polarization (ODNP) experiments have experienced a renaissance over the past decade, with a renewed focus on making the measurement quantitative. Although saturation of the electron spin Zeeman transition is central to the experiments, a quantitative model of saturation is not yet available. It currently is determined empirically. CW (continuous wave) powers on the order of 40–100 W [1–6] are varied until the maximum enhancement is observed. This causes heating effects, either of the sample [7–9] or changes in the components of the resonator [10]. Heating effects are deterrents to the use of ODNP as a quantitative technique, and make comparisons of different experimental conditions difficult. As a simple approximation, the saturation factor in the ODNP enhancement expression can be related to the electron spin longitudinal (T_{1e}) and transverse (T_{2e}) relaxation times as shown (Eqs. 1 and 2 [11]):

$$\varepsilon = 1 - \rho s f \frac{|\gamma_s|}{\gamma_I}, \tag{1}$$

$$s = \frac{\gamma_e^2 B_1^2 T_{1e} T_{2e}}{1 + \gamma_e^2 B_1^2 T_{1e} T_{2e}}, \tag{2}$$

where ε = enhancement in signal intensity, ρ = coupling factor, f = leakage factor, γ_s and γ_I are the electron and nuclear magnetogyric ratios, respectively, and B_1 is the microwave magnetic field that is applied to the unpaired electrons. Equation (2), derived from the Bloch equations, describes the case of a pure Lorentzian line. Although this lineshape is not encountered in practical ODNP experiments, Eq. (2) is useful for displaying trends in dependence of saturation on electron spin relaxation times.

The most commonly used radicals for solution ODNP are nitroxides. Interaction of the electron spin with the ^{14}N ($I = 1$) nucleus in the nitroxide produces a characteristic three-line spectrum. The splitting between each of the three lines is the isotropic hyperfine interaction, A_N. In a typical experiment, a single line of the nitroxide spectrum is pumped to saturate the electron spin Zeeman transition. ODNP enhancement is improved by transfer of saturation to all three nitrogen hyperfine lines. Saturating power can be transferred from one hyperfine manifold to another either by spin diffusion (Heisenberg exchange) [2] or nitrogen nuclear relaxation if $T_{1N} < T_{1e}$ [12]. For small nitroxides at room temperature or higher, tumbling correlation times, τ_R, are short enough that $T_{1N} \geq T_{1e}$ [13], so the predominant saturation transfer process is Heisenberg exchange. Heisenberg exchange increases proportional to concentration. For this reason, literature reports focusing on maximum ODNP enhancements have used concentrations of nitroxides from 1 mM upto 1 M [14, 15].

The renewed focus on solution ODNP has produced attempts to quantify the saturation, such as the report in 2007 [12]. These efforts would benefit from direct measurements of electron spin relaxation. If the components of the saturation factor for an ODNP experiment with a nitroxide could be measured, the ODNP experiment could be greatly improved. Calculation of the saturation factor combined with temperature corrected measurement of the leakage factor [9] would allow direct and quantitative calculation of ρ from ODNP enhancement data acquired at a single incident power or concentration—that is "single-shot" ODNP, as proposed in [16]. This would be an improvement over the traditional method of fitting many or all of the ODNP parameters and help overcome a major obstacle in the field of solution ODNP: comparison of enhancement and ρ values from one experiment to another. In addition, it would decrease the experiment time sufficiently to allow quick assessment of how the ODNP enhancement varies as a function of oxygen concentration, viscosity or oxidation/reduction status, furthering the utility of the measurement.

Studies of how T_{1e} and T_{2e} change over solution ODNP relevant concentration ranges are lacking, so the utility of equations such as those presented in [12] has not yet been realized. Typical measurements of the relaxation times of nitroxides in solution [17–21] or nitroxide spin-labels [22–25] have historically been made at concentrations below 1 mM, in an attempt to observe the "true" relaxation characteristics of the radicals. In this report, we present direct measurements of T_{1e} and T_{2e} upto 10–20.8 mM to overlap with experimental conditions of many ODNP experiments. The information that is gleaned from the high-concentration studies (T_{1e}, T_{2e}, T_{1HE}, T_{2HE}, and T_{1N}) is also applicable to recent ODNP studies using extremely low concentrations [26, 27]. The use of T_{1e}^* to denote the effective spin lattice relaxation time was introduced by Panagiotelis et al. [28] and we continue this distinction from the true spin–lattice relaxation time, T_{1e}.

1.1 Selection of Radicals

The two radicals used in this study (Fig. 1) represent the τ_R extremes for many small radicals in solution at room temperature across a wide range of solvents [18]. The radical tempol (TP) in toluene has a $\tau_R \sim 4$ ps, and the coupling factors in toluene and water have been shown to be very similar [29]. Toluene has ~40× lower dielectric
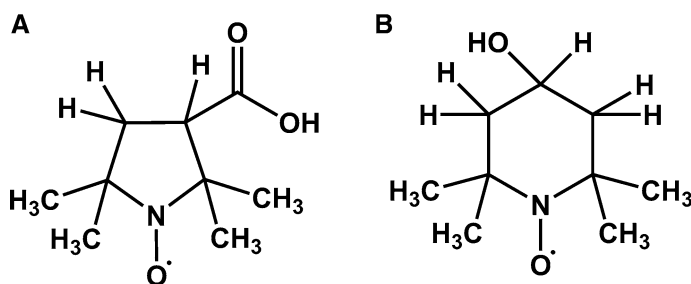
Fig. 1 Chemical structure of radicals studied. **a** Carboxy proxyl, CP, was studied in aqueous solution in the presence or absence of oxygen. **b** Tempol, TP, was studied in toluene in the absence of oxygen

loss in comparison to water ($\varepsilon_{Water} = 80.4$, $\varepsilon_{Toluene} = 2.4$ at 9.5 GHz), so sample heating is less of an issue. Toluene was the solvent of choice for a recent study of ODNP enhancement for a series of fullerene nitroxide derivatives [30]. The carboxy proxyl (CP) nitroxide in aqueous solution has a $\tau_R \sim 19$ ps [18]. CP has been shown to have low toxicity and long half-life in vivo [31] and its pharmacokinetics have been studied in tumors [32]. Esterified versions of CP can cross the blood brain barrier, and be converted to CP by enzymatic hydrolysis and trapped in the brain to provide information on O_2 in brain tissue [33]. Thus relaxation information for these radicals should be immediately applicable to general ODNP method development, and development of Overhauser enhanced MRI (OMRI), respectively.

2 Methods

2.1 Samples

CP (Sigma-Aldrich, Milwaukee WI) was dissolved in water to create a 10.4 mM stock solution, from which dilutions were made to final concentrations of 7.4, 5.3, 3.2, 2.1, 1.1, 0.5, 0.25, 0.125 and 0.025 mM. Samples were drawn up into Teflon tubing (0.97 mm i.d. thin wall, Zeus plastics), folded over once, sealed at each end with Critoseal tube sealant (Fisher Scientific) and placed in 4 mm OD quartz tubes. Using an additional thin Teflon tube N_2 gas was passed over the samples, which exchanged with oxygen through the walls of the Teflon tube. The N_2 purge was continued for a minimum of 60 min before data acquisition was started. To ensure removal of oxygen, values of T_{2e} were recorded beginning after 45 min of N_2 purge, and continued every 10 min until T_{2e} no longer increased and agreement between consecutive measured values was within < 3%. The same protocol has been previously used successfully with multi-frequency studies of low-concentration nitroxides [18, 20].

A stock solution of TP (Sigma-Aldrich, Milwaukee, WI) dissolved in toluene (Sigma-Aldrich, reagent grade) was prepared with a concentration of 10.3 mM. From this stock solution dilutions were made to final concentrations of 6.9, 5.2, 3.4, 2.1, 2. 0.5, and 0.025 mM. Between 300 and 400 µL of sample was loaded into 4 mm OD quartz EPR tubes (Wilmad Glass, NJ). To remove oxygen, each sample underwent a seven-cycle freeze–pump–thaw (FPT) procedure. The vacuum gauge reading during the last three freeze cycles was 5 mTorr. Each tube was then flame sealed.

When interpreting the absolute impact of O_2 on relaxation it should be noted that these experiments were performed in Denver where the altitude is about 5280 ft and the total atmospheric pressure is about 820 mbar (630 mTorr).

2.2 Echo Decay Measurements

Echo decay and inversion recovery measurements were performed on a Bruker Elexsys E580 spectrometer with a split ring resonator. Measurements of the phase

memory time, T_m, were made by spin echo decay with a two-pulse sequence $\pi/2$–τ–π–τ-echo, $\pi/2 = 20$ ns and initial $\tau = 100$ ns. For rapidly tumbling nitroxides in solution, $T_m \sim T_{2e}$ [20]. Two-step phase cycling was used for all measurements. Off-resonance measurements 100 G downfield from the $m_I = +1$ manifold showed a flat baseline, indicating that there are no instrumental artifacts that contribute to the on-resonance signals. For some of the shortest values of T_{2e}, the FID was measured using the $\pi/2$—FID sequence, which permits detection with shorter delay after the inverting pulse. A fit to the on-resonance FID was used to confirm the value of T_{2e} measured by echo decay.

In general there are multiple contributions to spin echo decay. For the conditions of this study—small molecules rapidly tumbling in fluid solution, the dominant contribution is the averaging of hyperfine lines due to Heisenberg exchange. Within the time window of the recorded echo decay, and given the finite signal-to-noise of the recorded decays, only a single exponential is needed to fit the data. Multiple exponentials do not improve the fit.

2.3 Inversion Recovery Measurements

Measurements for T_{1e}^* were made with three-pulse echo inversion recovery using the sequence π–T–$\pi/2$–τ–π–τ-echo with $\pi/2 = 20$ ns, constant $\tau = 100$ ns and initial $T = 100$ ns. At higher concentrations (> 5 mM), measurements also were made using FID-detected inversion recovery using the pulse sequence π–T–$\pi/2$—FID, which permits a shorter total time between the first pulse and the earliest point in the recovery curve than is possible for echo detection. Values of T_{1e}^* obtained by the two detection methods were in good agreement. Off-resonance experiments were made to confirm that there is no instrumental contribution to the recovery curves. For all inversion recovery experiments (echo or FID detection) a 4-step phase cycle program was used. Most data sets were acquired with initial $T = 100$ or 200 ns and 256 increments in T of 100 or 200 ns. As discussed in the Supplementary Information (Fig. S1), the time constants extracted from fits to the high-concentration (~ 5 mM) data were sensitive to selection of the initial delay T. For both radicals, several experiments were performed in which initial T, step size and data collection window length were varied.

2.4 Saturation Recovery Measurements

Saturation recovery experiments were performed on a modified Bruker Elexsys E500T X-Band spectrometer equipped with a Tektronix AWG70002A arbitrary waveform generator and a locally designed microwave bridge that will be reported later (J. McPeak, R.W. Quine, S.S. Eaton, G.R. Eaton, unpubl.). Measurements were made using a 5-loop-4-gap resonator [34], with an unloaded Q of 2600 and a microwave efficiency of 3.2 G/W$^{1/2}$. A saturating pulse of ~ 800 mW and 60 μs was used followed by a low power observation pulse of ~ 25 μW and a repetition time of 200 μs. Off-resonance spectra were subtracted to minimize instrumental artifacts.

Each saturation recovery data point reported here is the result of ten replicate measurements recorded sequentially without disruption of the spectrometer tuning and sample placement.

2.5 Fitting of Experimental Data

Fitting of time constants to spin echo and inversion recovery data was done with the Plot Fitting tool in Matlab (MathWorks, Cambridge, MA) using equations for single or double-exponential decays (Eqs. 3 and 4).

$$Y(t) = Y_0 e^{-t/T_x}, \tag{3}$$

$$Y(t) = \left(A_0 e^{-\frac{t}{T_{1A}}} \right) + \left(B_0 e^{-\frac{t}{T_{1B}}} \right), \tag{4}$$

where Y_0, A_0 and B_0 are amplitudes at time zero, $t = 2\tau$ for spin echo or T for inversion recovery and $T_x = T_{1e}*$ or T_{2e}. Under certain circumstances (described below) the inversion recovery data were better described with a two-exponential fit (Eq. 4). The 95% confidence interval for each fit value was used to create error bars on each point in the plots of relaxation time vs. concentration. Saturation recovery data were fit to a two-component exponential model with Bruker Xepr software that uses Eq. 4. Errors were based on standard deviation for replicate measurements.

For the T_{2e} measurements the fits were single exponential, as expected for fast tumbling radicals in solution at room temperature. For inversion recovery experiments, single and double-exponential fits were compared for each data set (Fig. S2). To report that a two-component fit was better than a single-component fit, two criteria had to be met. First, 95% confidence intervals had to be $\leq 10\%$ for each component. For cases where the $T_{1e}*$ fit to the experimental data was clearly a single exponential (< 1 or > 7 mM), a forced two-exponent fit to the data had confidence intervals from $> 10\%$ to several hundred % of the fit value. Second, for data sets for which the fit was judged to be better for two exponentials there was a significant improvement in the R^2 value of the fit and reduction in the root-mean-square-error (RMSE) compared with that for the single exponential. The ratio of the RMSE for the single exponent fit (SE_{RMSE}) to the RMSE for the two-exponent fit (DE_{RMSE}) is shown in Fig. S3. To report a two-exponential fit, a criterion of $SE_{RMSE}/DE_{RMSE} > 2$ was used. As an additional criterion for selection of a double-exponential rather than single-exponential fit, data were analyzed using two locally written programs, MULTIFIT and uniform penalty method, UPEN [35, 36], which report the goodness of fit with an SNR parameter—the higher the SNR the better the fit. The UPEN program fits the data with a distribution of time constants. These additional analyses confirmed the appropriateness of the two-component models for concentrations between 1 and 5 mM.

2.6 Modeling of Relaxation Times

The interpretation of relaxation times is based on previously reported expressions (Eqs. 5–11) for the following contributions:

a. Heisenberg exchange

$$\frac{1}{T_{1HE}} = \frac{1}{T_{2HE}} = \kappa_{HE}[R],$$

(5)

where κ_{HE} is the Heisenberg exchange rate constant, and $[R]$ is the concentration of the radical in millimole/liter.

b. Electron spin relaxation [13, 18]

For a rapidly tumbling nitroxide

$$\frac{1}{T_{1e}} = \frac{1}{T_1^{SR}} + \frac{1}{T_{1e}^{END}},$$

(6)

$$\frac{1}{T_1^{SR}} = \frac{\sum_{i=1}^{3}(g_i - g_e)^2}{9\tau_R},$$

(7)

where $i = x, y, z$ and g_e is 2.0023.

$$\frac{1}{T_{1e}^{END}} = \frac{2}{9}I(I+1)\sum_i (A_i - \overline{A})^2 \left(\frac{\tau_R}{1 + (\omega_e \tau_R)^2}\right)$$

(8)

where I is the nitrogen nuclear spin.

c. Nitrogen nuclear relaxation [13]

$$\frac{1}{T_{1N}} = \frac{1}{T_{1n}^{END}} + \frac{1}{T_{1n}^{sd}},$$

(9)

$$\frac{1}{T_{1n}^{END}} = \frac{1}{20}\sum_i (A_i - \overline{A})^2 \left[\frac{\tau_R}{1 + (\omega_a \tau_R)^2} + \frac{\left(\frac{7}{3}\right)\tau_R}{1 + (\omega_e \tau_R)^2}\right],$$

(10)

where A_i is a component of the nitrogen nuclear hyperfine in angular frequency units, $\bar{A}$ is the average nitrogen hyperfine, ω_e is the electron Zeeman frequency in angular units, and $\omega_a = \bar{A}/2$.

$$\frac{1}{T_{1n}^{sd}} = R_{1n}^{sd}, \max\left(\frac{2\omega_n\tau_R}{1+(\omega_n\tau_R)^{1.5}}\right)^{\frac{1}{4}},$$ (11)

where R_{1n}^{sd},max $=0.13$ MRad/s and ω_n is the nuclear Zeeman frequency in angular units.

3 Results

3.1 Spin Echo Measurements of T_{2e}

Relaxation times T_{2e} were measured for CP in water in the absence and presence of oxygen (Fig. 2a) and for TP in toluene in the absence of oxygen (Fig. 2b). Previous measurements of T_{2e} for CP in deoxygenated aqueous solution by spin echo decay were 430 ns at 0.5 mM [18], 570 ns at 0.25 mM [20] and 680 ns for 0.025 mM [37], for $m_I=0$. These literature values are in excellent agreement with the data in Fig. 2a. For the nitroxide tempone (4-oxo-2,2,6,6-tetramethylpiperidinyloxy), which has a structure that is similar to TP, a previous X-band measurement found $T_{2e}=340$ ns in 0.5 mM toluene [18].

When the concentration of CP is low, removal of O_2 has a large impact on T_{2e} (Fig. 2a). The impact of oxygen on T_{2e} is significant up to about 3 mM. At 3 mM and higher concentrations, T_{2e} for CP is nearly independent of oxygen. This observation agrees with the understanding that T_{2e} is dominated by Heisenberg exchange at concentrations >3 mM [38]. The limiting value of T_{2e} at high concentration is about 50 ns for all cases, irrespective of radical, solvent or the presence/absence of oxygen (Fig. 2). The limiting value of T_{2e} is reached at about 5 mM for TP in toluene and slightly greater than 7 mM for CP in aqueous solution. The higher radical
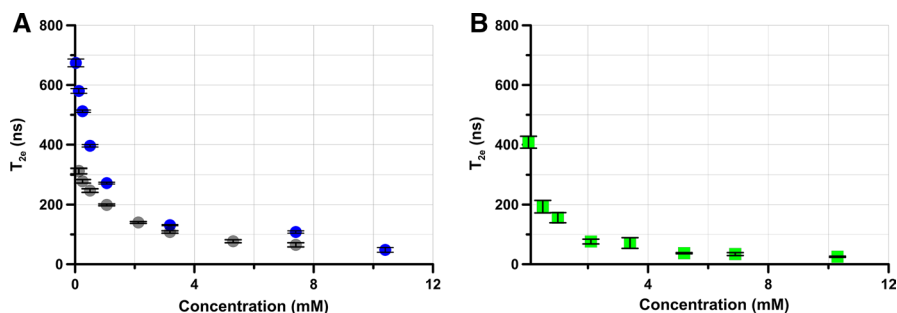
Fig. 2 T_{2e} for CP and TP in solution. **a** T_{2e} for CP in water in the absence (blue circle) or presence (grey circle) of oxygen. Data from $m_I=0$ are plotted. **b** T_{2e} for TP in toluene in the absence of oxygen (green square) (color figure online)

concentration that is required to achieve the limiting relaxation rate in water than in toluene is attributed to the higher viscosity of water and therefore lower collision rates. Collision rates for CP may also be decreased by the negative charge on the carboxyl group for the partially dissociated carboxylic acid.

The T_{2e} data for both radicals were used to calculate spin exchange rates. The effect on EPR linewidth (or T_{2e}) from Heisenberg spin exchange is given by Eq. 12 [39–41]:

$$\frac{1}{T_{2e}}(\text{mM}) = \frac{1}{T_{2e}}(0) + \kappa_{HE}[R],\tag{12}$$

where $T_{2e}^{-1}(0)$ is the value at the lowest concentration (25 µM), where spin exchange is negligible. By subtracting the contribution of $T_{2e}^{-1}(0)$ from each value at higher concentration, the spin exchange rates, $\kappa_{HE}[R]$ can be calculated. The slope of the plot of $\kappa_{HE}[R]$ vs. concentration (Fig. 3) yields Heisenberg exchange rates of $(2.0\pm0.1)\times10^6$ mM^{-1} s^{-1} for CP in water, and $(3.6\pm0.6)\times10^6$ mM^{-1} s^{-1} for TP in toluene. The Heisenberg exchange rates calculated from T_{2e} measurements from each nitrogen manifold were in good agreement with each other for both radicals (Fig. S7).

3.2 Inversion Recovery Experiments

The time constant obtained by a single-exponential fit to the inversion recovery data is designated at T_{1e}*. The concentration dependence of T_{1e}* for CP in water was measured in the absence or presence of oxygen (Fig. 4a). In the presence of oxygen, the inversion recovery curves fit well with a single exponential at all concentrations studied, and T_{1e}* decreased to a limiting value of 200 ns at concentrations of 1 mM. A similar pattern has been observed previously using continuous wave saturation up to 4 mM [42]. In the absence of oxygen, T_{1e}* decreases from 900 to
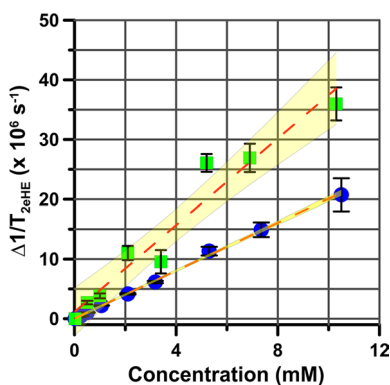

Fig. 3 Heisenberg exchange rates calculated from the concentration dependence of T_{2e}. Data shown are for the $m_I=0$ line for CP and TP in the absence of oxygen. A linear fit to the data gives a slope of $(2.0\pm0.1)\times10^6$ mM^{-1} s^{-1} for CP in water (blue circle, $R^2=0.999$) and $(3.6\pm0.6)\times10^6$ mM^{-1} s^{-1} (green square, $R^2=0.946$) for TP in toluene. Both fits show a region of 95% confidence interval in yellow. The uncertainties are based on the range of slopes that fit the data within the 95% confidence intervals (color figure online)
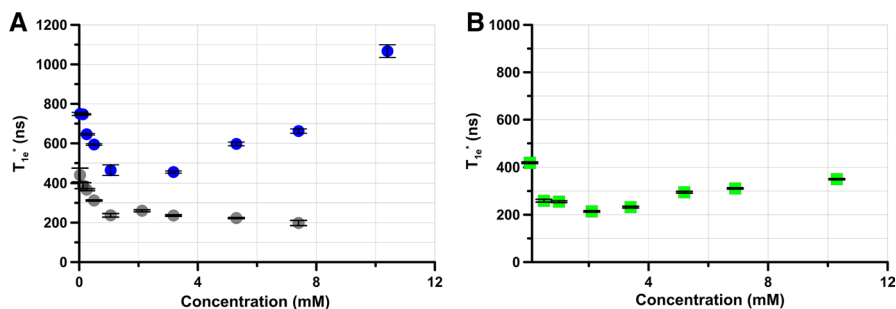
Fig. 4 Concentration dependence of $T_{1e}*$ at room temperature. **a** CP in water in the absence (blue circle) or presence (grey circle) of oxygen. **b** TP in toluene in the absence of oxygen (green square). Data from $m_I=0$ are plotted (color figure online)

400 ns as concentration increases from 0.25 to 1 mM. At concentrations greater than 1 mM, $T_{1e}*$ *increases* as concentration increases from 1 to 10 mM. The concentration dependence of $T_{1e}*$ for TP in toluene (Fig. 4b) is similar to that for CP in water (Fig. 4a), with values of $T_{1e}*$ again increasing at concentrations > 1 mM.

At concentrations between about 1 and 7 mM, the fits to the data for both CP and TP are better for the sum of two exponentials (Eq. 4) than for a single exponential (Fig. S2). This pattern at intermediate radical concentrations was observed for each of the three hyperfine lines (Fig. S4). For both CP and TP the concentration dependence of the component with the smaller time constant is similar to that for T_{2HE} and therefore this time constant is assigned as T_{1HE} (Eq. 5, Fig. 5). For CP the component with the larger time constant is between 600 and 800 ns and was assigned to T_{1e}, based on the agreement with the previously reported value of 630 ns for the $m_I=0$ line [18]. For TP the longer time constant is about 350 ns, which is similar to the value of 360 ns reported for T_{1e} for tempone in toluene [18]. The slopes
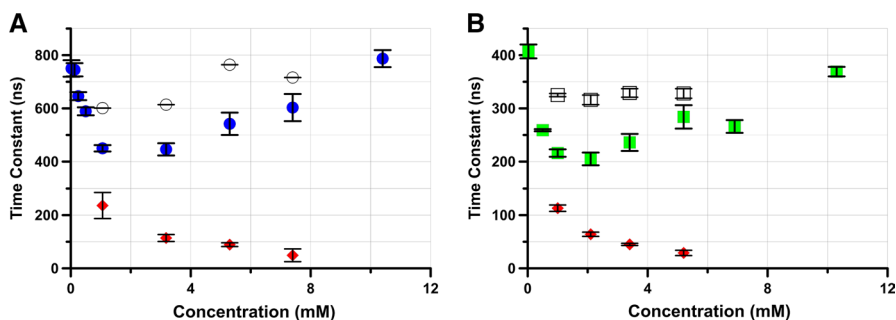

Fig. 5 Time constants for CP and TP in the absence of O_2 obtained by fits to single and double exponentials. T_1* is shown for both CP (blue circle) and TP (green square) for comparison to time constants extracted at intermediate concentrations. At concentrations between about 1 and 7 mM the fits to the sum of a long component (circle, square) and short component (red diamond) are better than for a single exponential. Data for $m_I=0$ are plotted. Note the y-axis for CP is twice that of TP to display differences in T_{1e} (color figure online)

of plots of T_{1HE}^{-1} as a function of concentration give values of $\kappa_{HE} = (2.4 \pm 0.7) \times 10^6$ and $(6.0 \pm 0.7) \times 10^6$ mM^{-1} s^{-1} for CP and TP, respectively (Fig. S5), and there was good agreement for κ_{HE} calculated from all three hyperfine manifolds (Fig. S8). The values of κ_{HE} for CP obtained from $1/T_{1HE}$ and $1/T_{2HE}$ agree, within experimental uncertainty. The values of κ_{HE} for TP obtained from $1/T_{1HE}$ and $1/T_{2HE}$ differ by about a factor of 1.5, which is greater than the estimated uncertainties.

3.3 Long-Pulse Saturation Recovery Experiments

In previous studies of rapidly tumbling nitroxides in 0.5 mM solution, the spin magnetization recovery time constants obtained from inversion recovery and saturation recovery experiments agreed within 10% [18]. Relaxation time constants measured by inversion recovery may be impacted by spectral diffusion and Heisenberg exchange arising from collisions. At the much higher concentrations studied here, collisions play a larger role than at lower concentrations. Long-pulse saturation recovery measurements allow spectral diffusion and collisions to equilibrate the populations of the spin manifolds and the recovery time is expected to be T_{1e} [43]. Saturation recovery experiments were carried out on concentrations up to 20.8 mM (Fig. 6). Fits to the experimental data for CP and TP were better for two components than for one (Fig. S6). For CP the time constants are $(3.8 \pm 0.8) \times 10^3$ and $(0.60 \pm 0.08) \times 10^3$ ns (Fig. 6a). For TP (Fig. 6b) the two time constants are $(7.9 \pm 0.5) \times 10^3$ and $(0.31 \pm 0.03) \times 10^3$ ns.

For both TP and CP the short components obtained by the saturation recovery experiment match well with the low-concentration (25 μM) measurements of $T_{1e}*$ and with the literature values for T_{1e}. In the absence of saturation transfer mechanisms (like HE) at these very low concentrations, $T_{1e}* = T_{1e}$. Values of T_{1N} were calculated as a function of tumbling correlation times using Eqs. (9–11). For CP in aqueous solution, τ_R in the range of 18–20 ps results in T_{1N} about 2.7×10^3 ns, which is within a factor of two of the value of the longer time constant obtained by long-pulse saturation recovery. For TP in toluene, τ_R in the range of 4–6 ps results in T_{1N}
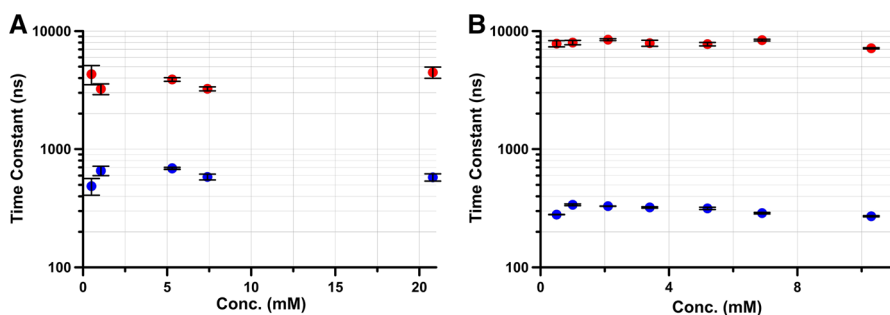
Fig. 6 Relaxation times obtained by long-pulse saturation recovery. For CP (**a**) the two time constants are $(3.8 \pm 0.8) \times 10^3$ ns (red circle) and $(0.60 \pm 0.08) \times 10^3$ ns (blue circle). For TP (**b**) the two time constants are $(7.9 \pm 0.5) \times 10^3$ ns (red circle) and $(0.31 \pm 0.03) \times 10^3$ ns (blue circle) (color figure online)

of 8×10^3–6×10^3 ns, which is similar to the longer time constant obtained by long-pulse saturation recovery.

4 Discussion

It is widely recognized that determination of the ODNP saturation factor requires knowledge of T_{1e}, T_{2e}, T_{1N}, Heisenberg exchange rate, and microwave B_1 at the sample [44, 45]. In some cases, direct calculation of the saturation factor has been reported [44]. In this paper, we report direct measurements of several contributions to electron spin relaxation as a function of concentration and seek a physical interpretation of the relaxation rates. We, and others [44], assume that the Heisenberg exchange rate can be derived from T_{2e} (some others have used the line width in place of direct measurement of T_{2e}). This assumption would only be valid if there are no aggregation processes that could impact relaxation as a function of concentration.

4.1 Heisenberg Exchange

In our discussion, we assume simple Brownian diffusion following prior work in this field, starting with Pake and Tuttle in 1959 [46], and continued by Freed in 1969 [47] and the latest papers by Salikhov, Bales, and Peric [48–52]. For low-viscosity fluid solutions, we do not see a need for a more elaborate model of collisions. Linear dependence of linewidth on concentration has been observed by other investigators, such as [53] and more recently in [54] over the concentration range of 2–50 mM. Over about six decades of study, several investigators have explored relative contributions of exchange and dipolar interactions for a wide range of radical types, including charges, solvents, viscosity, temperature, and concentration. Interpretations invoke nearly every physical phenomenon implied by other studies, such as solvent cage effects, initial collision encounters and re-encounters, distance dependence of orbital overlap for exchange, stereochemistry and mutual orientation of collisions, and relative rotations as well as translational diffusions. Most of the studies have examined effects on the CW EPR line shape and width.

In prior work we observed that the contribution to nitroxide relaxation from T_{1HE} is negligible at concentrations up to about 0.5 mM, based on agreement between inversion recovery and saturation recovery measurements [18]. That proposal is consistent with the observation in this study that at 25 μM $T_{1e}* = T_{1e}$. Contributions to relaxation combine as the sum of reciprocals of the time constants. The non-monotonic concentration dependence of $T_{1e}*$ is observed because for low concentrations, T_{1HE}^{-1} is too small relative to T_{1e}^{-1} to make a significant contribution to $T_{1e}*^{-1}$. As concentration increases and T_{1HE} decreases (T_{1HE}^{-1} increases), $T_{1e}*$ is dominated by T_{1HE} and decreases with increasing concentration. At higher concentrations T_{1HE} decreases to the point where it is too short to be extracted from the magnetization recovery curve. Concurrent with the decrease of T_{1HE} (increase in T_{1HE}^{-1}) is transfer of saturating power from one nitrogen manifold to the other, such that at the highest concentrations $T_{1e}* \sim T_{1e}$ again. This explains the increase in $T_{1e}*$ from 1 up to

10 mM. The values of T_{1e} measured by long-pulse saturation recovery are in good agreement with the values of T_{1e} obtained by the two-component fits to the inversion recovery experiments. Previous data at 34 GHz for CP at 0.5 mM were characterized by a two-exponent fit of ca. 1.6 and 0.5 µs [55]. The calculated value of T_{1N} at 34 GHz for $\tau_R = 19$ ps is 5 µs, which is much longer than 1.6 µs, so the time constant of 1.6 µs was assigned as T_{1e}. This left the 0.5 µs time constant unassigned, and this time constant may have been T_{1HE}.

The concentration dependence of T_{2e} and T_{1e} were used to calculate the exchange rate constant κ_{HE}. In units of 10^6 mM^{-1} s^{-1}, Heisenberg exchange rates based on concentration dependence of line widths have been reported as ranging from <1 to about 7 for several species in water and some organic solvents. The exchange rate for charged radicals depends on added electrolyte concentration [28, 47, 56]. The effect of bimolecular collision on exchange rate depends on specific solvation of the radical and on orientation. In addition, charged radicals may not come within the required proximity for efficient exchange due to charge repulsion between colliding molecules, and solvent interactions (i.e., hydrogen bonding). Literature values of κ_{HE} are shown in Table 1. Our values of κ_{HE} for TP in toluene are similar to previously reported values for TP in toluene and for structurally similar tempone in toluene. If it is assumed that the spin exchange interaction is in the strong exchange regime, then κ_{HE} is predicted to be inversely proportional to viscosity [57]. Thus, the approximate factor of two decrease in κ_{HE} between TP in toluene and CP in water is consistent with the factor of two increase in viscosity. Values of κ_{HE} for low molecular weight semiquinones in dimethoxyethane, which has viscosity similar to that of toluene, are also similar to values obtained for the nitroxides (Table 1).

It is usually assumed that the contributions of Heisenberg exchange to $1/T_{2e}$ equally contribute to $1/T_{1e}$. Values of κ_{HE} for CP in water obtained from $1/T_{2e}$ and

Table 1 Comparison of Heisenberg exchange constants, κ_{HE}

Sample	Molar mass (g/mol)	Solvent	Viscosity, η, cP[a]	κ_{HE} from $1/T_{2e}$	κ_{HE} from $1/T_{1e}$	Refence
TP	172	Toluene	0.50	3.9[b]	5.8[b]	This work
TP	172	Toluene	0.50		5.1	[30]
Tempone-d$_{16}$	170	Toluene	0.50	3.63		[40]
CP	186	Water	1.0	2.0[b]	2.5[b]	This work
Tempone	170	Water	1.0	2.2		[44]
1,4-Benzosemiquinone	108	Dimethoxyethane	0.5	2.98		[57]
2,3,5,6-Tetramethyl-1,4-benzosemiquinone	164	Dimethoxyethane	0.5	3.52		[57]

In units of 10^6 mM^{-1} s^{-1}, measured at temperatures between 15 and 20 °C

[a]Viscosity at 20 °C

[b]Average for three nitrogen hyperfine lines

$1/T_{1e}$ are similar, and probably within experimental error. Values of κ_{HE} for TP in toluene obtained from $1/T_{2e}$ and $1/T_{1e}$ differ by about 50%. This difference is larger than the uncertainties estimated from the reproducibility of the data. However, there may be systematic errors that are difficult to estimate when the values of T_{1e} and T_{2e} at the highest radical concentrations studied are 20–50 ns and the instrumental dead time is about 100 ns, which will require further investigation.

Salikhov, Bales, Peric, and coworkers in extensive series of papers provided insight into the contributions of exchange and dipole–dipole interactions based on CW EPR line shape analysis of nitroxide radicals. Simulations were performed over a wide range of concentrations. The theory includes resolved ^{15}N and ^{14}N splittings and unresolved proton hyperfine couplings, charge effects, coherence transfer, models of collisions, re-encounters, strength of the exchange interactions and many other parameters. Many of these ideas are summarized in [52]. A primary focus in these papers has been the use of the dispersive components of the CW spectra to measure spin exchange, and to distinguish exchange and dipolar contributions. Our present work uses pulsed EPR rather than CW EPR to separate the Heisenberg exchange contributions to T_1 and T_2, using pulse amplitudes that encompass the unresolved proton hyperfine lines.

Almost all of our measurements were for concentrations lower than those for which simulations of line shapes were performed in Ref. [48–51]. Inherent in our analyses are conclusions from prior work that for nitroxides spin exchange is strong [52] and that spin dephasing rates are linearly dependent on concentration [54]. Prior discussions of the theory of exchange and dipolar interactions assumed no dependence on mutual orientation of the colliding particles. Values of K_{ex} measured in water "are consistently found to be smaller than in other solvents, by a factor of 0.50–0.71" [49]. The Heisenberg exchange rates assumed in the calculations of [51] were smaller than we found experimentally or in the literature.

4.2 Predictions for Frequency Dependence

The experiments reported in this paper were performed at X-band (9.5 GHz) which is widely used for EPR. T_{1HE} is expected to be independent of frequency for CP and TP radicals. The T_{1e} and T_{2e} values for CP and for tempone (similar in structure to TP) have been previously shown to be *dependent on* frequency from 0.35 T (9.5 GHz, X-band) up to 1.2 T (34.5 GHz, Q-band) [18]. From 0.35 T down to 0.010 T relaxation times are nearly frequency *independent* with a small increase in $1/T_{1e}$ near 40 mT (1-2 GHz, L-band) due to the presence of a thermally activated process [18, 58]. For values of τ_R of 4 ps up to about 200 ps small changes in τ_R can affect the frequency dependence of T_{1e} and T_{2e} significantly.

Modern solution ODNP has been performed from 1.5 mT [38] up to 9.2 T [15]. For a given tumbling correlation time, averaging of anisotropic components will be less effective as frequency increases from 9.5 GHz, resulting in decreasing values of T_{2e} from 9.5 to 34 GHz. For τ_R in the range of 4 ps to 19 ps the dominant contributions to T_{1e} are spin rotation (Eq. 7) which is frequency independent. Modulation of the electron–nuclear dipole (END) interaction (Eq. 8) is frequency dependent for

EPR frequencies > 9.5 GHz. Note that the impact of the END mechanism diminishes from 9.5 to 34 GHz, such that T_{1e} at 34 GHz is *almost* entirely determined by spin rotation. The net result of both contributions is an increase in T_{1e} (decrease in T_{1e}^{-1}) from 9.5 to 34 GHz. As noted in [18], the few experimental reports of decreasing T_{1e} (increasing T_{1e}^{-1}) at frequencies greater than 34 GHz are not yet well understood.

Empirical observation of T_{1N} has been reported for spin-labels [25, 59, 60], but less widely applied to free radicals in solution [30]. T_{1N} is weakly frequency dependent (Eq. 9–11). As frequency is increased from 9.5 to 95 GHz calculated values of T_{1N} increase from about 6–12 μs for $\tau_R = 5$ ps and from about 3–5 μs for $\tau_R = 19$ ps. To date we are not aware of any ODNP experiments that have incorporated the frequency dependence of T_{1e}, T_{2e} or T_{1N} into the design of ODNP experiment or interpretation of enhancement results.

5 Summary

ODNP is becoming a powerful spectroscopic technique for the study of water dynamics in biochemical [61] and materials [62–64] research, in addition to its promising applications when used to enhance magnetic resonance imaging experiments. Careful study and characterization of the saturation factor is the last remaining barrier to quantitative measurement, which will allow full realization of the technique's power. Towards that end, the relaxation times T_{1e}, T_{1HE}, T_{1N}, T_{2e}, and T_{2HE} have been measured for two radicals in two different solvents at 9.5 GHz using well established pulse techniques that could be reproduced in other laboratories interested in ODNP experiments. The next goal will be use of the quantitative ODNP saturation parameters in direct calculation of the saturation factor to facilitate quantitative single-shot ODNP.

References

1. T.R. Carver, C.P. Clichter, Phys. Rev. **102**, 975–980 (1956)
2. R.D. Bates, W.S. Drozdoski, J. Chem. Phys. **67**, 4038–4044 (1977)
3. D.J. Lurie, I. Nicholson, J.S. McLay, J.R. Mallard, Appl. Magn. Reson. **3**, 917–925 (1992)
4. D. Grucker, T. Guiberteau, B. Eclancher, J. Chambron, R. Chiarelli, A. Rassat, G. Subra, B. Gallez, J. Magn. Reson. **106**, 101–109 (1995)
5. D.M. TonThat, M.P. Augustine, A. Pines, J. Clarke, Rev. Sci. Instrum. **68**, 1527–1531 (1997)
6. M. Alecci, D.J. Lurie, J. Magn. Reson. **138**, 313–319 (1999)
7. P.J.M. Van Bentum, G.H.A. van der Heijden, J.A. Villanueva-Garibay, A.P.M. Kentgens, Phys. Chem. Chem. Phys. **13**, 17831–17840 (2011)
8. E.V. Kryukov, K.J. Pike, T.K. Tam, M.E. Newton, M.E. Smith, R. Dupree, Phys. Chem. Chem. Phys. **13**, 4372–4380 (2011)
9. J.M. Franck, A. Pavlova, J.A. Scott, S. Han, Prog. Nucl. Magn. Reson. Spectrosc. **74**, 33–56 (2013)
10. J.R. Biller, K.F. Stupic, J.M. Moreland, Magn. Reson. Chem. **56**, 1–11 (2017)

11. E. Ravera, C. Luchinat, G. Parigi, J. Magn. Reson. **264**, 78–87 (2016)
12. B.D. Armstrong, S. Han, J. Chem. Phys. **127**, 104508 (2007)
13. B.H. Robinson, D.A. Haas, C. Mailer, Science **263**, 490–493 (1994)
14. S. Garcia, J.H. Walton, B. Armstrong, S. Han, M.J. McCarthy, J. Magn. Reson. **203**, 138–143 (2010)
15. P. Neugebauer, J.G. Krummenacker, V.P. Denysenkov, G. Parigi, C. Luchinat, T.F. Prisner, Phys. Chem. Chem. Phys **15**, 6049–6056 (2013)
16. J.R. Biller, R. Barnes, S. Han, Curr. Opin. Colloid Interface Sci. **33**, 72–85 (2018)
17. H.B. Elajaili, J.R. Biller, M. Tseitlin, I. Dhimitruka, V.V. Khramtsov, S.S. Eaton, G.R. Eaton, Magn. Reson. Chem. **53**, 280–284 (2015)
18. J.R. Biller, H. Elajaili, V. Meyer, G.M. Rosen, S.S. Eaton, G.R. Eaton, J. Magn. Reson. **236**, 47–56 (2013)
19. J.R. Biller, V.M. Meyer, H. Elajaili, G.M. Rosen, S.S. Eaton, G.R. Eaton, J. Magn. Reson. **225**, 52–57 (2012)
20. J.R. Biller, V. Meyer, H. Elajaili, G.M. Rosen, J.P.Y. Kao, S.S. Eaton, G.R. Eaton, J. Magn. Reson. **212**, 370–377 (2011)
21. V. Meyer, S.S. Eaton, G.R. Eaton, Appl. Magn. Reson. **45**, 993–1007 (2014)
22. J.J. Yin, J.B. Feix, J.S. Hyde, Biophys. J. **58**, 713–720 (1990)
23. J.S. Hyde, W. Froncisz, C. Mottley, Chem. Phys. Lett. **110**, 621–625 (1984)
24. J.B. Feix, J.J. Yin, J.S. Hyde, Biochemistry **26**, 3850–3855 (1987)
25. W. Froncisz, T.G. Camenisch, J.J. Ratke, J.R. Anderson, W.K. Subczynski, R.A. Strangeway, J.W. Sidabras, J.S. Hyde, J. Magn. Reson. **193**(2), 297–304 (2008)
26. E. Bordignon, H. Brutlach, L. Urban, K. Hideg, A. Savitsky, A. Schnegg, P. Gast, M. Engelhard, E.J. Groenen, K. Möbius, H.J. Steinhoff, Appl. Magn. Reson. **37**, 391–403 (2010)
27. A. Doll, E. Bordignon, B. Joseph, R. Tschaggelar, G. Jeschke, J. Magn. Reson. **222**, 34–43 (2012)
28. I. Panagiotelis, I. Nicholson, M.A. Foster, J.M.S. Hutchison, Magn. Reson. Med. **46**, 1223–1232 (2001)
29. N. Enkin, G.Q. Liu, I. Tkach, M. Bennati, Phys. Chem. Chem. Phys. **16**, 8795–8800 (2014)
30. N. Enkin, G.Q. Liu, M.D. Gimenez-Lopez, K. Porfyrakis, I. Tkach, M. Bennati, Phys. Chem. Chem. Phys. **17**, 11144–11149 (2015)
31. N. Kosem, T. Naganuma, K. Ichikawa, N.P. Morales, K. Yasukawa, F. Hyodo, K. Yamada, H. Utsumi, Free Radic. Bio. Med. **53**, 328–336 (2012)
32. F. Hyodo, K. Yasukawa, K. Yamada, H. Utsumi, Magn. Reson. Med. **56**, 930–943 (2006)
33. S.R. Burks, N. Jiahong, S. Muralidharan, A. Coop, J.P.Y. Kao, G.M. Rosen, Bioconjugate Chem. **19**, 2068–2071 (2008)
34. G.A. Rinard, R.W. Quine, S.S. Eaton, G.R. Eaton, W. Froncisz, J. Magn. Reson. A **108**, 71–81 (1994)
35. G.C. Borgia, R.J.S. Brown, P. Fantazzini, J. Magn. Reson. **132**, 65–77 (1998)
36. G.C. Borgia, R.J.S. Brown, P. Fantazzini, J. Magn. Reson. **147**, 273–285 (2000)
37. J.R. Biller, V.M. Meyer, H. Elajaili, S.S. Eaton, G.R. Eaton, in *53rd Rocky Mountain Conference on Analytical Chemistry* (Snowmass, USA, 24–28 July 2011), Poster #156
38. M.D. Lingwood, I.A. Ivanov, A.R. Cote, S. Han, J. Magn. Reson. **204**, 56–63 (2010)
39. D. Marsh, Biol. Magn. Reson. **8**, 255–303 (1989)
40. J. Gorchester, J.H. Freed, J. Chem. Phys. **88**, 4678–4693 (1988)
41. A.E. Stillman, R.N. Schwartz, J. Magn. Reson. **22**, 269–277 (1976)
42. M. Giordano, M. Martinelli, L. Pardi, S. Santucci, Mol. Phys. **42**, 523–531 (1981)
43. S.S. Eaton, G.R. Eaton, in *Handbook of EPR spectroscopy: fundamentals and methods*, ed. by D. Goldfarb, S. Stoll (John Wiley & Sons, Chichester, 2018), pp. 175–192
44. M.-T. Türke, I. Tkach, M. Reese, P. Höfer, M. Bennati, Phys. Chem. Chem. Phys. **12**, 5893–5901 (2010)
45. M. Gafurov, V. Denysenkov, M.J. Prandolini, T.F. Prisner, Appl. Magn. Reson. **43**, 119–128 (2012)
46. G.E. Pake, T.R. Tuttle, Phys. Rev. Lett. **3**, 423–425 (1959)
47. M.P. Eastman, R.G. Kooser, M.R. Das, J.H. Freed, J. Chem. Phys. **51**, 2690–2709 (1969)
48. K.M. Salikhov, Appl. Magn. Reson. **38**, 237–256 (2010)
49. K.M. Salikhov, A.Y. Mambetov, M.M. Bakirov, I.T. Khairuzhdinov, R.T. Galeev, R.B. Zaripov, B.L. Bales, Appl. Magn. Reson. **45**, 911–940 (2014)
50. K.M. Salikhov, Appl. Magn. Reson. **47**, 1207–1227 (2016)
51. K.M. Salikhov, M.M. Bakirov, R.T. Galeev, Appl. Magn. Reson. **47**, 1095–1122 (2016)

52. B.L. Bales, M. Peric, Appl. Magn. Reson. **48**, 175–200 (2017)
53. S. Ablett, M.D. Barratt, F. Franks, J. Solut. Chem. **4**, 797–807 (1975)
54. D. Merunka, M. Peric, J. Phys. Chem. B **121**, 5259–5272 (2017)
55. J. R. Biller, Electronic Theses and Dissertations, University of Denver (2014)
56. M.P. Eastman, G.V. Bruno, J.H. Freed, J. Chem. Phys. **52**, 2511–2522 (1970)
57. D.S. Leniart, H.D. Connor, J.H. Freed, J. Chem. Phys. **63**, 165–199 (1975)
58. K. Kundu, D.R. Kattnig, B.Y. Mladenova, G. Grampp, R. Das, J. Phys. Chem. B **119**, 4501–4511 (2015)
59. J.J. Yin, J.B. Feix, J.S. Hyde, Biophys. J. **53**, 525–531 (1988)
60. J.J. Yin, J.S. Hyde, J. Magn. Reson. **74**, 82–93 (1987)
61. I. Kaminker, R. Barnes, S. Han, Methods Enzymol. **564**, 457–483 (2015)
62. J.H. Ortony, S.H. Choi, J.M. Spruell, J.N. Hunt, N.A. Lynd, D.V. Krogstad, V.S. Urban, C.J. Hawker, E.J. Kramer, S. Han, Chem. Sci. **5**(1), 58–67 (2014)
63. J.H. Ortony, C.Y. Cheng, J.M. Franck, R. Kausik, A. Pavlova, J. Hunt, S. Han, New J. Phys. **13**(1), 015006 (2011)
64. J. Song, O.H. Han, S. Han, Angew. Chem. Int. Ed. **54**(12), 3615–3620 (2015)

Affiliations

Joshua R. Biller[1,3] 🔘 · **Joseph E. McPeak**[2] 🔘 · **Sandra S. Eaton**[2] 🔘 ·
Gareth R. Eaton[2] 🔘

1   Physical Measurement Laboratory, National Institute of Standards and Technology, 325 Broadway, Boulder, CO 80305, USA

2   Department of Chemistry and Biochemistry, University of Denver, Denver, CO 80210, USA

3   Present Address: TDA Research, Inc., Golden, CO 80403, USA